ACS OMEGA

http://pubs.acs.org/journal/acsodf

Article

Preparation of a GO/MIL-101(Fe) Composite for the Removal of Methyl Orange from Aqueous Solution

Zhuannian Liu, Wenwen He,* Qingyun Zhang, Habiba Shapour, and Mohammad Fahim Bakhtari

Cite This: *ACS Omega* 2021, 6, 4597−4608

Read Online

ACCESS | Metrics & More | Article Recommendations

ABSTRACT: The composite material graphene oxide (GO)/MIL-101(Fe) was prepared by a simple one-pot reaction method. MIL-101(Fe) grown on the surface of a GO layer was confirmed by scanning electron microscopy (SEM), X-ray diffraction (XRD), Fourier transform infrared spectroscopy (FTIR), and thermogravimetric analysis (TGA). The adsorption performance and the mechanism of MIL-101(Fe) and GO/MIL-101(Fe) for methyl orange (MO) were studied. The results have shown that the adsorption capacity of GO/MIL-101(Fe) for MO was significantly better than that of MIL-101(Fe), and its capacity was the highest when 10% GO was added. The Langmuir specific surface areas of MIL-101(Fe) and GO/MIL-101(Fe) were 1003.47 and 888.289 $m^2 \cdot g^{-1}$, respectively. The maximum adsorption capacities of MO on MIL-101 (Fe) and 10% GO/MIL-101 (Fe) were 117.74 and 186.20 $mg \cdot g^{-1}$, respectively. The adsorption isotherms were described by the Langmuir model, and the adsorption kinetic data suggested the pseudo-second order to be the best fit model. GO/MIL-101(Fe) can be reused at least three times.

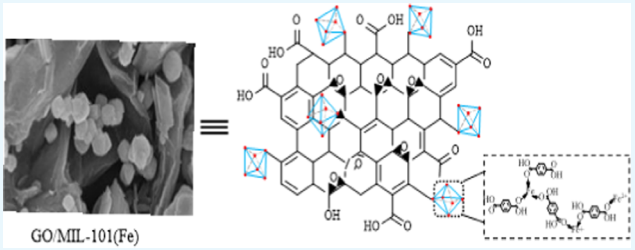

1. INTRODUCTION

The pollutants in the aqueous environment are mainly organic dyes, and most of them can exist in the environment for a long time. In addition, they are able to enter the human body through the food chain and cause a serious negative effect on human health.[1] It is estimated that more than 50 billion tons of dyes are used in the dyeing process every year, and the annual consumption of reactive dyes accounts for about 30% of the globally used dyes. On the other hand, during the dyeing process, 20−60% of reactive dyes are inevitably lost,[2] and methyl orange (MO, which is an anionic dye[3]) is one of them. MO is widely used in the textile, food, paper, pharmaceutical, and printing industries, and due to its −N═N− structure and low biodegradability, it may result in numerous human health and environmental problems.[4] Therefore, it is essential to remove MO from water systems to reduce its negative impact on the environment. Hence, developing new materials or technologies that can effectively remove these pollutants is the top priority.[5] There are many methods for removing organic dyes from industrial wastewaters, such as chemical degradation, biodegradation, and physical adsorption;[6] among various methods, adsorption has many advantages like low cost, effective treatment, and being eco-friendly,[7] which gradually becomes one of the most feasible methods for treating water pollutants.[8]

Metal−organic frameworks (MOFs), also known as porous coordination polymers or porous coordination networks (PCNs), are metal ions or metal clusters and organic ligands with multiple binding sites (N or O atoms), where a self-assembled single-component crystal complex finally forms a two-dimensional (2D) or three-dimensional (3D) infinitely extending coordination network in space.[9] An MOF has not only ultrahigh surface area, large pore volume, and adjustable surface properties (unsaturated metal sites) but also excellent structural properties (pore size and geometry).[10] There are many types of metal−organic framework materials, for example, MIL-101(Cr),[11] MIL-88(Fe),[12] MIL-53(Al),[13] cobalt-based material ZIF-8[14] (ZIF = zeolite imidazole salt skeleton), and copper-based material Cu-BTC,[15] which can be applied to various fields, including gas storage and separation, photocatalysis, drug delivery, and other fields.[16,17] Recently, MOFs have attracted widespread attention in the treatment of pollutants in wastewater. The iron-based metal−organic framework material, i.e., MIL-101(Fe), is one of the most representative materials in the MIL-n series. MIL-101(Fe) is a multistage pore structure, and its large pore diameter provides excellent adsorption capacity. According to Kholdeeva and Skobelev et al.,[18] MIL-101(Fe) is more stable in water since it can bind active components such as guest molecules and metal nanoparticles to confine it in its pores or in a cage to improve

Received: October 19, 2020
Accepted: January 27, 2021
Published: February 8, 2021

its adsorption performance. Thanh and Phuong et al.[19] showed through an experiment that the maximum adsorption capacity of Fe-MIL-101 for Pb(II) is much higher than that of MIL-101. The surface functional group of Fe-MIL-101 adsorbing Pb(II) is considered to be the formation of hydroxyl groups on the iron oxide group. MIL-101(Fe) can be fixed functional materials or composite unique products using suitable materials to improve its ability to adsorb and remove pollutants in wastewater.[20] Hamedi and Zarandi et al.[21] synthesized a magnetic metal−organic framework (MOF) composite (MIL-101(Fe)@PDopa@Fe_3O_4) for the excellent adsorption capacities of methyl red (MR) and malachite green (MG). Hamedi and Trotta et al.[22] synthesized MIL-101(Fe)@Fe_3O_4@AC via the hydrothermal method to adsorb rhodamine, which showed relatively high efficiency for RhB. Hence, in this study, MIL-101(Fe) was synthesized with graphene oxide (GO) to improve its adsorption capacity. There are few researchers who have studied the core−shell structure composite (GO@MIL-101(Fe)) that is applied in photocatalysis; however, none has definitely shown and described the structure of the composite (GO/MIL-101(Fe)). This study focused on MIL-101(Fe) as a super small active polyhedron that can be synthesized with GO and grown on the surface of the material layers with strong stable properties and a sheet structure; the number of its active sites are relatively limited for the removal of organic pollutants from wastewater.

Graphene oxide (GO) is a strong stable material of the representative graphene derivatives. There are some oxygen-containing functional groups in the center and edges of the graphene oxide sheet.[23] The existence of these groups causes graphene oxide to be bonded by the van der Waals force between the layers. Some researchers have studied different number of layers of graphene oxide sheets by the ultrasonically exfoliated treatment method,[24−27] providing a lamellar structure that made MIL-101(Fe) grow easily on the surface of GO's layers. Meanwhile, many studies found that GO can be modified with other materials or on its surface and it can be synthesized with other materials to fabricate materials with dual advantage, obtaining the aimed purpose and a complementary product. Xiuna Jia and Pan Zhao et al.[28] synthesized MIL-101(Cr)@GO via the solvothermal method and applied it as an effective adsorbent for dispersive micro-solid-phase extraction. The experimental results show that MIL-101(Cr) is clearly improved when combined with GO. Similarly, Li and Miao et al.[29] prepared Cu-BTC@GO composites by mechanochemical synthesis and its experimental results revealed that compared with Cu-BTC, the adsorption performance and water stability of Cu-BTC@GO are improved, and even the removal rate of toluene can reach 98.2%.

Therefore, in this paper, MIL-101(Fe) was synthesized with GO. *n*GO/MIL-101(Fe) (*n* is the mass ratios of GO to GO, terephthalic acid, and $FeCl_3·6H_2O$) as an adsorbent was prepared via the solvothermal method for the removal of MO. The effects of adsorption parameters such as the pH of the solution, the dosage of the adsorbent, and the temperature and recycling of the adsorbent were investigated, Besides, adsorption kinetics, isotherm, and thermodynamics studies were also conducted. Compared to MIL-101(Fe), the adsorption capacity of GO/MIL-101(Fe) for the removal of MO in wastewater obviously increased. In addition, it makes the application of MOFs more extensive in wastewater treatment.

2. EXPERIMENTAL SECTION

2.1. Materials and Instrumentation. *2.1.1. Materials.* Ferric chloride hexahydrate ($FeCl_3·6H_2O$), terephthalic acid (H_2BDC), and *N*,*N*-dimethylformamide (DMF) used in this study were purchased from Sinopharm Chemical Reagent Co. Graphite powder was purchased from Tianjin Damao Chemical Reagent, and methyl orange was purchased from Tianjin Tianhe Chemical Reagent Factory. All chemical reagents were of analytical grade, and aqueous solutions were prepared with deionized water.

2.1.2. Instrumentation. The concentration of MO was quantified by a UV−visible spectrophotometer (TU-1810SPC, Universal Analysis, Beijing) at 465 nm. X-ray powder diffraction (XRD) analysis was performed using an XD-3 (Universal Analysis, Beijing) diffractometer using Cu Kα radiation (40 kV, 40 mA, λ1/4 0.15418 nm) to determine the structure and composition of the fabricated material. Raman spectra of materials were recorded by a Raman spectrometer (inVia Reflex, RENISHAW, U.K.). A Fourier transform infrared (FTIR) spectrometer (550s, Perkin Elmer) was used to analyze the chemical structure of the sample. A N_2 adsorption equipment (JW-BK122W, Beijing) was applied to analyze the surface area and pore-size distribution. The morphology analysis of the samples was performed by a scanning electron microscope (FE-SEM S4800, Japan). Thermogravimetric analysis (TGA) data were obtained from TGA/DSC 1 STAR^e System (Mettler Toledo); the samples were heated to 800 °C at a rate of 10 °C·min^{-1} in a nitrogen atmosphere. The size distribution of the particles was measured by a Bettersize2600 laser particle size instrument. The ζ-potential of the samples was obtained by a JS94 Microelectrophoresis apparatus (Zeta potentiostat).

2.2. Preparation of MIL-101(Fe) and GO/MIL-101(Fe). The MIL-101(Fe) material[30] was synthesized by the solvothermal method. In this study, 0.427 g of terephthalic acid and 1.461 g of $FeCl_3·6H_2O$ were dissolved in 30 mL of *N*,*N*-dimethylformamide and then stirred continuously for 1 h at room temperature. Then, the mixed solution was transferred into a reaction kettle lined with poly(tetrafluoroethylene) and placed in an oven at 120 °C for a constant temperature reaction for 24 h. After that, the reaction kettle was cooled to room temperature and the obtained sample was centrifuged and washed repeatedly with DMF and anhydrous ethanol. Then, the sample was dried in an oven at 70 °C and finally activated in a vacuum drier at 150 °C for 10 h.

The preparation of the GO material is divided into three stages. At 0−4 °C, 1 g of the graphite powder was added to 23 mL of concentrated H_2SO_4, and then 3 g of $KMnO_4$ and 0.5 g of $NaNO_3$ were added and continuously stirred for 60 min till the color became dark green. Then, the sample was stirred at three different temperatures: medium temperature (at 35 °C stirred for 3 h), high temperature (at 85 °C stirred for 15 min while 46 mL of DI water was slowly dropped into the sample), and room temperature (10 mL of H_2O_2 was added to the sample and stirred for 1 h). Then, the sample was centrifuged at a high speed, and a 5% dilute HCl solution was added to the sample and immersed overnight. Then, the sample was washed with a 5% HCl solution five times and rinsed repeatedly with deionized water. The pH of the supernatant solution was kept close to neutral and dried in an oven at 60 °C for 12 h.

https://dx.doi.org/10.1021/acsomega.0c05091
ACS Omega 2021, 6, 4597−4608

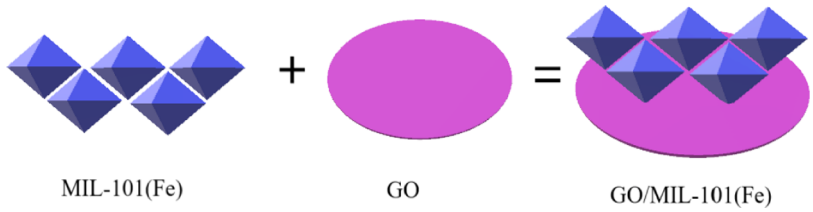

Figure 1. MIL-101(Fe) and GO/MIL-101(Fe) model diagram.

The preparation processes of the GO/MIL-101(Fe) composite material are shown in Figure 1. To prepare GO/MIL-101(Fe), 0.427 g of terephthalic acid and 1.461 g of $FeCl_3 \cdot 6H_2O$ were dissolved in 30 mL of *N*,*N*-dimethylformamide and stirred at room temperature for 1 h. Then, a certain amount of GO was added into 6 mL of ethanol and ultrasonically dispersed for 30 min and later added to the above solution. The mixed solution was regularly ultrasonicated for 20 min until the two solutions were mixed together completely. Later, the mixture was placed in a reaction kettle and reacted at a constant temperature of 120 °C for 24 h. After the reaction kettle was cooled to room temperature, the obtained sample was centrifuged and washed repeatedly with *N*,*N*-dimethylformamide and absolute ethanol. Then, the sample was dried in an oven at 70 °C and activated by a vacuum drier at 150 °C for 10 h. The mass ratios of GO to GO, terephthalic acid, and $FeCl_3 \cdot 6H_2O$ were 2, 5, 10, 15, and 20% and were recorded as 2%GO/MIL-101(Fe), 5%GO/MIL-101(Fe), 10%GO/MIL-101(Fe), 15%GO/MIL-101(Fe), and 20%GO/MIL-101 (Fe), respectively.

2.3. Adsorption Experiments. *2.3.1. Influence of Adsorbents on Adsorption Performance.* To know the mass ratio that had the higher adsorption performance, 50 mg of MIL-101(Fe) and GO/MIL-101(Fe) were added into 100 mL (100 mg·L^{-1}) of the MO solution and continuously shaken at 25 °C for 3 h. Then, the sample was filtered and the concentration of MO was analyzed by a spectrophotometer.

2.3.2. Adsorption Thermodynamics. In the equilibrium experiment, 50 mg of MIL-101(Fe) and GO/MIL-101(Fe) were added into 100 mL (20, 30, 50, 100, 200, and 300 mg·L^{-1}) of the MO solution and continuously shaken at 25 °C for 3 h. Subsequently, the sample was filtered and the concentration of MO was analyzed by the spectrophotometer.

2.3.3. Influence of the pH Value, Dosage, and Temperature on Adsorption. A certain amount of MIL-101(Fe) and GO/MIL-101(Fe) was added to 100 mL (100 mg·L^{-1}) of the MO solution. Different pH values were observed using 0.1 M NaOH and 0.1 M HCl solutions at different temperatures by continuously shaking the sample for 3 h. Then, the sample was filtered and the concentration of MO was analyzed.

The amount of adsorption is determined by the following equation

$$q_e = \frac{(C_0 - C_e)V}{m} \quad (1)$$

where q_e is the adsorption capacity at equilibrium (mg·g^{-1}); C_0 is the initial concentration of MO in solution (mg·L^{-1}); C_e is the equilibrium concentration of MO (mg·L^{-1}); V is the volume of the MO solution (L); and m is the mass of the adsorbent (g).

3. RESULTS AND DISCUSSION

3.1. Characterization of MIL-101(Fe) and GO/MIL-101(Fe). *3.1.1. XRD and Raman Analysis.* The XRD patterns of GO, MIL-101(Fe), and GO/MIL-101(Fe) materials are presented in Figure 2. As seen from the figure, MIL-101 (Fe)

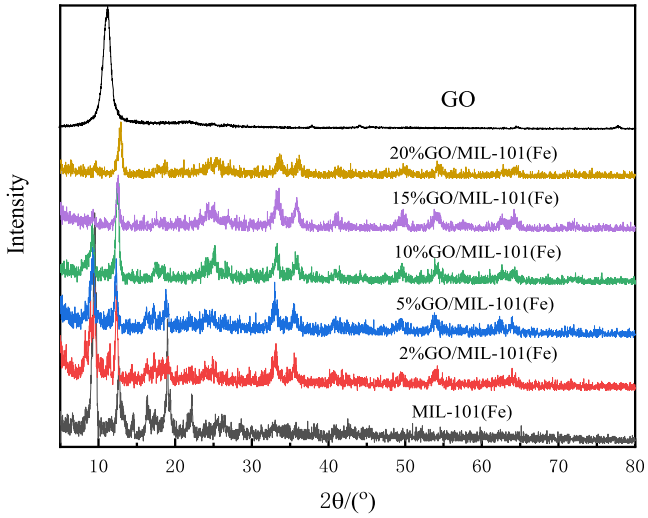

Figure 2. XRD patterns of GO, MIL-101(Fe), and (2, 5, 10, 15, and 20%) GO/MIL-101(Fe).

has obvious absorption peaks at 2θ values of 5.18, 8.78, 9.36, 18.98, and 23.7°, corresponding to the (111), (220), (311), (511), and (852) crystal planes. GO has a diffraction peak at a 2θ of 11.2°, corresponding to the (002) crystal plane, which implied that GO was synthesized successfully. In the diffraction spectrum of GO/MIL-101 (Fe), the characteristic peak of GO's multilayer structure basically disappears since the GO in the composite material is mainly a single-layer structure, which may be due to the high dispersion of GO after ultrasonic treatment, which was reported in previous studies.[28,31] As the amount of GO in the composite increases, the strength of the characteristic peak of MIL-101(Fe) becomes weak gradually. The strength of the characteristic peak of MIL-101(Fe) was the weakest until 20% GO was added, which demonstrated that MIL-101(Fe) was successfully synthesized with GO. The Raman spectra of GO, MIL-101(Fe), and GO/MIL-101(Fe) are shown in Figure 3. The G and D bands of GO are located at 1600 and 1353 cm^{-1}, respectively. The G band corresponds to the vibration of sp^2 carbon atoms, while the D band is related to the disordered carbon of the edge and defect sites.[32,33] Several bands of MIL-101(Fe) are mainly related to the organic ligands, the bands at 1433 and 1145 cm^{-1} are assigned to C═O in the carboxylic group and the C−C bond of the benzene ring, respectively, and the band appeared at 860 cm^{-1} is ascribed to the vibrations of C−H and the benzene ring. The characteristic bands of GO and MIL-101(Fe) appear

https://dx.doi.org/10.1021/acsomega.0c05091
ACS Omega 2021, 6, 4597−4608

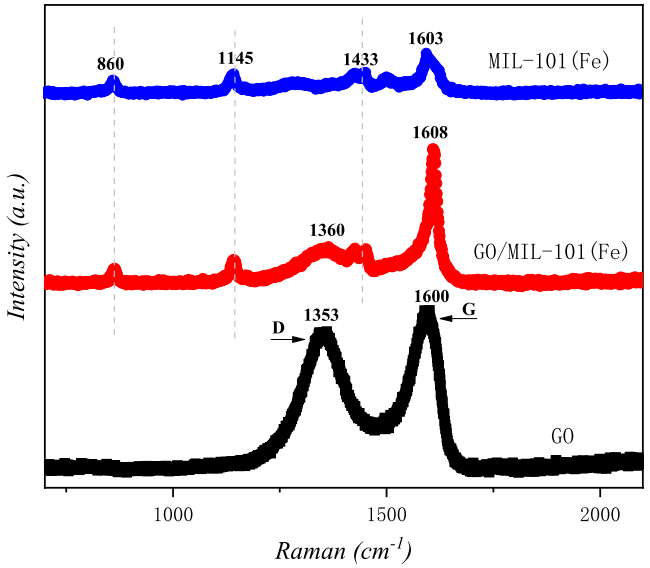

Figure 3. Raman spectra of the as-prepared samples.

in the GO/MIL-101(Fe) composite and the red Raman shift (D and G bands) of GO in the composite is located at 1360 and 1608 cm^{-1}, indicating that the interaction between GO and MIL-101(Fe) is in line with the result of XRD.

3.1.2. FTIR Spectra Analysis. The FTIR spectra of the MIL-101(Fe) and GO/MIL-101(Fe) materials are shown in Figure 4. As for graphene oxide, the characteristic peaks of GO above

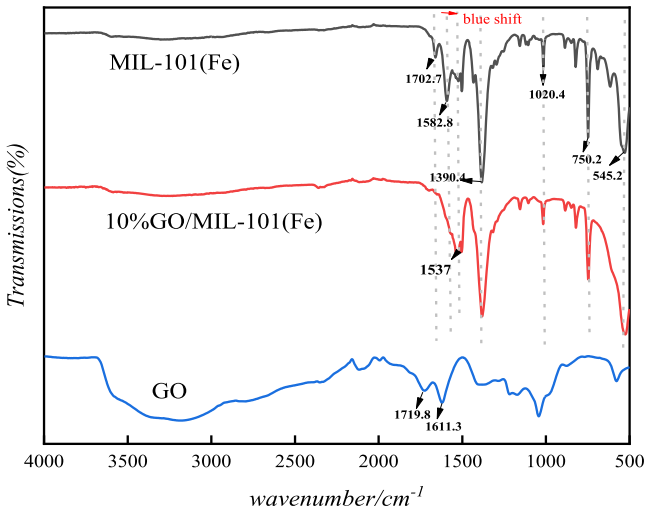

Figure 4. FTIR spectra of MIL-101(Fe), 10% GO/MIL-101(Fe), and GO.

3000 cm^{-1} and near 1719 cm^{-1} are related to the oxygen functional groups (such as −OH and C═O in carboxyl groups) on the GO surface.[34] The peaks of graphene oxide at 1611 cm^{-1} and at around 1100 cm^{-1} are related to −OH in adsorbed water and alkoxy C−O, respectively.[35] The characteristic peaks of MIL-101-(Fe) were located at 545, 750, 1020, 1390, 1582, and 1702 cm^{-1}, which proved that MIL-101(Fe) was successfully synthesized. The peak at 545 cm^{-1} was assigned to the Fe−O bond,[22] which appeared in both MIL-101(Fe) and GO/MIL-101(Fe), and the peaks at 750 and 1020 cm^{-1} were assigned to C−H bending vibrations and C−O−C, respectively.[36] The peaks located at 1390 and 1582 cm^{-1} corresponded to the symmetric and asymmetric vibrations of O−C═O, and the peak at 1702 cm^{-1} corresponded to the C═O bond in carboxyl groups and was in line with the reported literature.[37,38] The peaks at 3000 and 1719 cm^{-1} of the composite disappeared as the −OH and −COOH groups on the surface of GO have reacted with MIL-101(Fe). The peak of MIL-101(Fe) in the composite at 1582 cm^{-1} disappeared and the one at 1390 cm^{-1} became slightly weak, which may be because GO agglomerates limited the formation of MIL-101(Fe) in the composite. The peak of GO/MIL-101(Fe) at 1702 cm^{-1} disappeared and the one at around 1537 cm^{-1} is the blue shift of the O−C═O bond and has been even strengthened, which demonstrated that MIL-101(Fe) was successfully grown on the surface area of GO. The characteristic peaks of MIL-101(Fe) mostly appeared in the GO/MIL-101(Fe) composite, indicating that the crystal structure of MIL-101(Fe) remained in the composite.

3.1.3. SEM Analysis. The SEM images of MIL-101(Fe) and GO/MIL-101(Fe) materials are presented in Figure 5, and accordingly, it is found that MIL-101(Fe) is a regular polyhedron, as shown in Figure 5a,b. The aggregates of GO/MIL-101(Fe) and MIL-101(Fe) nanocomposites look completely different. It can be seen that after mixing 10% GO, MIL-101(Fe) was grown on the surface of GO. As the amount of GO increased, the crystal size decreased gradually. GO in the lamellar layer may limit the formation of MIL-101(Fe) polyhedra, and thus MIL-101(Fe) crystals on the surface of GO become smaller and more irregular. The particle-size distribution of MIL-101(Fe) and GO/MIL-101(Fe) is shown in Table 1.

3.1.4. Brunauer−Emmett−Teller (BET) Surface Areas and Pore Structure Analysis. The nitrogen adsorption−desorption isotherms and pore-size distributions of MIL-101(Fe) and GO/MIL-101(Fe) are given in Figure 6 and Table 2. It can be seen from Figure 6 that MIL-101(Fe) shows very high N_2-saturated adsorption capacity, and the N_2-saturated adsorption amount of 10% GO/MIL-101(Fe) drops obviously. It can be seen from Figure 6a that the MIL-101(Fe) material shows a similar type I adsorption−desorption isotherm, which proves that it has a typical microporous structure and has a uniform pore-size distribution.[36] Table 2 describes the specific surface area and pore structure parameters of MIL-101(Fe) and GO/MIL-101 (Fe) materials. It can be seen that the specific surface area of 10% GO/MIL-101(Fe) decreased compared to MIL-101(Fe), which indicates that the doping of GO can regulate the specific surface area of GO/MIL-101(Fe) composites. The decrease of the specific surface area was mainly due to the minimal pore structure of GO, which relatively reduces the number of pores per unit mass of the composite material,[32] and accumulation of GO in the composite material can reduce the specific surface area of the composite material. In addition, when GO was added, GO agglomerated in the reaction system and made organic ligands difficult to coordinate with Fe^{3+} ions, which may fail to prevent the formation of the crystal structure of MIL-101(Fe). Therefore, the specific surface area of the GO/MIL-101(Fe) composite was reduced.

3.1.5. TGA Analysis. The TGA analysis of MIL-101(Fe) and GO/MIL-101(Fe) is shown in Figure 7. The weight loss of MIL-101(Fe) occurs at 50−330 °C due to the evaporation of moisture and the elimination of free terephthalates in the pores of MIL-101(Fe). Subsequently, the significant weight loss from 330 to 650 °C is attributed to the decomposition of coordinated organic ligands as a result of the breakdown of

https://dx.doi.org/10.1021/acsomega.0c05091
ACS Omega 2021, 6, 4597−4608

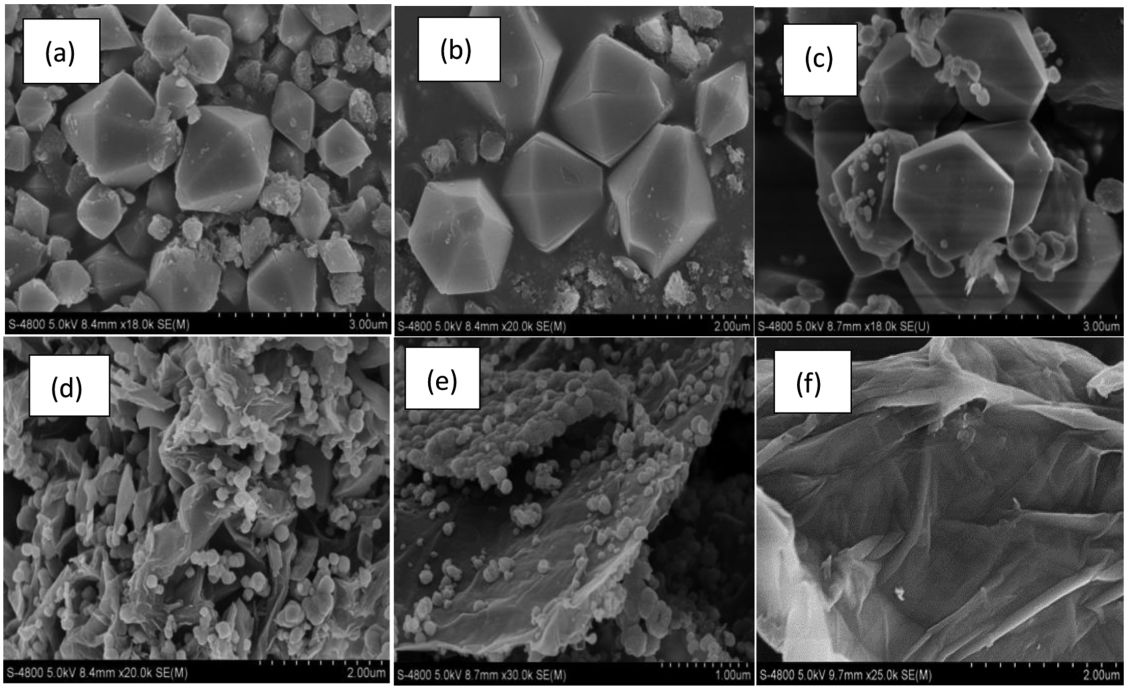

Figure 5. SEM analysis of MIL-101(Fe) (a, b),10% GO/MIL-101(Fe) (c, d), 20% GO/MIL-101(Fe) (e), and GO(f).

Table 1. Particle-Size Distribution of MIL-101(Fe) and GO/MIL-101(Fe)

samples	D_{av} (μm)	D_{10} (μm)	D_{50} (μm)	D_{90} (μm)
MIL-101(Fe)	25.96	1.181	13.31	69.23
GO/MIL-101(Fe)	9.179	0.986	4.923	24.15

Table 2. Surface Area and Pore Structure Parameters of MIL-101(Fe) and GO/MIL-101(Fe)

samples	BET surface area ($m^2 \cdot g^{-1}$)	Langmuir surface area ($m^2 \cdot g^{-1}$)	pore volume ($cm^3 \cdot g^{-1}$)	pore diameter (nm)
MIL-101(Fe)	607.93	1003.47	0.43	2.63
GO/MIL-101(Fe)	542.69	888.289	0.40	2.73

the framework, and at around 800 °C, the framework collapses. In general, the GO/MIL-101(Fe) composite has shown a similar thermal degradation process compared to pure MIL-101(Fe). However, GO/MIL-101(Fe) showed a slight weight loss due to the existence of GO at temperatures from 600 to 800 °C.

3.2. Effect of Adsorbents on Adsorption Performance. The effect of MIL-101(Fe) and the different mass ratios

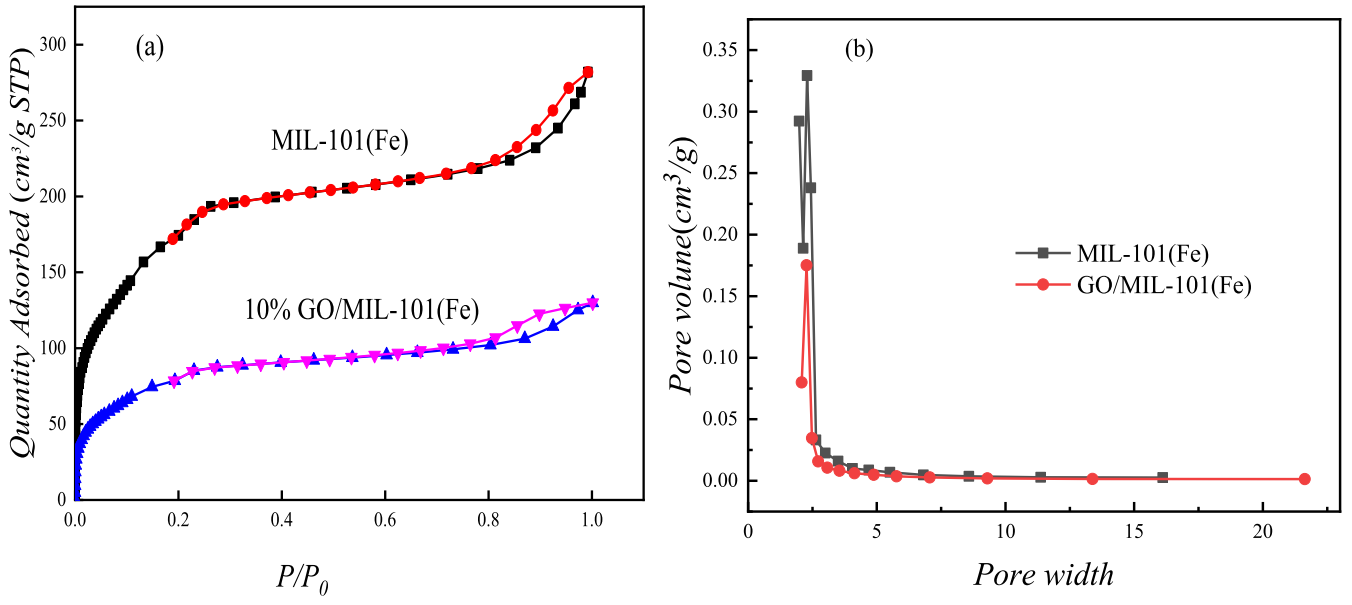

Figure 6. Nitrogen isotherm analysis of MIL-101(Fe) and GO/MIL-101(Fe) (a) and pore-size distribution analysis of MIL-101(Fe) and GO/MIL-101(Fe) (b).

https://dx.doi.org/10.1021/acsomega.0c05091
ACS Omega 2021, 6, 4597−4608

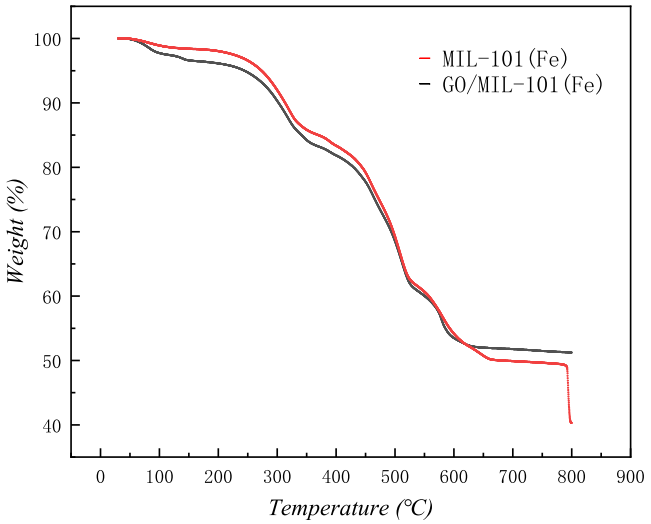

Figure 7. TG curves of MIL-101(Fe) and GO/MIL-101(Fe).

of GO/MIL-101(Fe) on the removal of MO is shown in Figure 8. It can be seen from Figure 8 that the adsorption

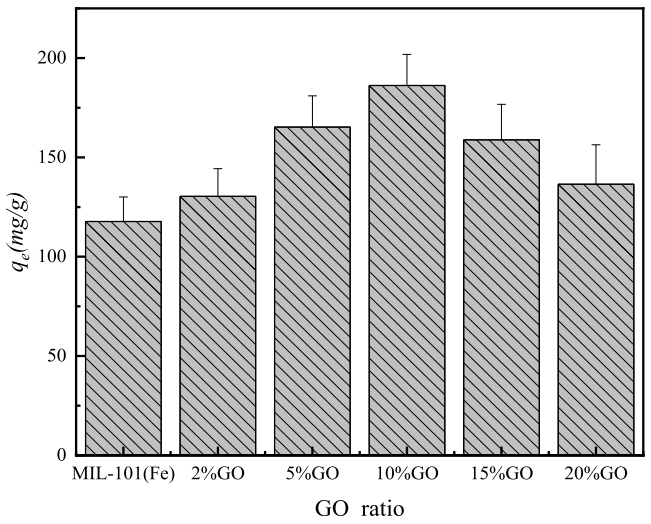

Figure 8. Effect of the GO ratio on the adsorption of MO onto MIL-101(Fe) and GO/MIL-101(Fe).

capacity of MO on GO/MIL-101(Fe) has been significantly improved and the adsorption capacity of 10% GO/MIL-101(Fe) is the highest. As the mass ratio of graphene oxide increased continuously, the adsorption performance of MO decreased gradually. Due to the presence of a large amount of GO that occupied the pores of the MIL-101(Fe) material, the pores of the composite and the surface active sites of the adsorbent decreased, and thus the adsorption of MO was also reduced. 10% GO/MIL-101(Fe) was denoted as GO/MIL-101(Fe) in all subsequent experiments.

3.3. Adsorption Kinetics. The effects of time on the adsorption of MIL-101(Fe) and GO/MIL-101(Fe) are shown in Figure 9. It can be seen from Figure 9 that the adsorption capacity of MO by MIL-101(Fe) and GO/MIL-101(Fe) increased rapidly before 30 min. This was due to the large specific surface area of MIL-101(Fe) and GO/MIL-101(Fe) and a large number of active adsorption sites on the surface. With the increase of time, most of the adsorptive active sites

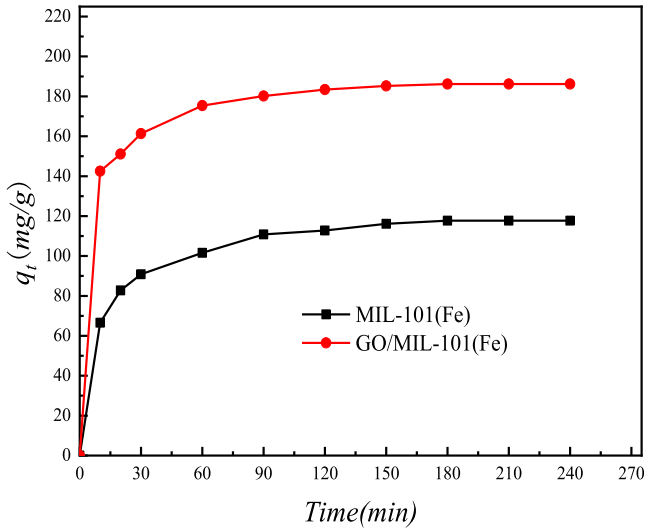

Figure 9. Effect of time on the adsorption of MO onto MIL-101(Fe) and 10% GO/MIL-101(Fe).

were gradually occupied and the adsorption rate slowed down after 180 min, finally reaching the equilibrium. The adsorption capacity of 10% GO/MIL-101(Fe) for MO was 68% higher than that of MIL-101(Fe).

To better study the relationship between the adsorption processes of MIL-101(Fe) and GO/MIL-101(Fe) for the removal of MO, the Lagergren model was used to analyze its adsorption kinetics. The first-order reaction kinetic model and pseudo-second-order kinetic model can be calculated to determine the adsorption rate constant. The linear form of the Lagergren first-order model is represented as follows

$$\log(q_e - q_t) = \log q_e - \frac{k_1}{2.303}t \quad (2)$$

where q_e and q_t (mg·g^{-1}) are the amounts adsorbed at equilibrium and at time t (min), respectively, and k_1 (min^{-1}) is the rate constant for the Lagergren first-order model.

The kinetic data were further analyzed using pseudo-second-order kinetics expressed as follows

$$\frac{t}{q_t} = \frac{1}{k_2 q_e^2} + \frac{1}{q_e}t \quad (3)$$

where k_2 (g·mg^{-1}·min^{-1}) is the rate constant of the pseudo-second-order model.

The pseudo-secondary curves of MIL-101(Fe) and GO/MIL-101(Fe) for MO adsorption are shown in Figure 10. The kinetic parameters obtained for the Lagergren primary and pseudo-secondary models (where q_{ec} is the calculated equilibrium adsorption amount) are listed in Table 3. For the pseudo-second-order kinetic model, the regression correlation coefficients (R^2) of the adsorption of MIL-101(Fe) and GO/MIL-101(Fe) for MO were greater than the R^2 of the Lagergren first-order kinetic model and were 0.9970 and 0.9993, respectively. The equilibrium adsorption capacity data calculated by pseudo-second-order kinetics ($q_{e.c}$) is also close to the equilibrium adsorption capacity in the experiment. The amount of equilibrium adsorption calculated according to the formula was close to the equilibrium adsorption capacity obtained in the experiment, which indicated that the adsorption behavior of MIL-101(Fe) and GO/MIL-101(Fe) materials for methyl orange suggested the

https://dx.doi.org/10.1021/acsomega.0c05091
ACS Omega 2021, 6, 4597−4608

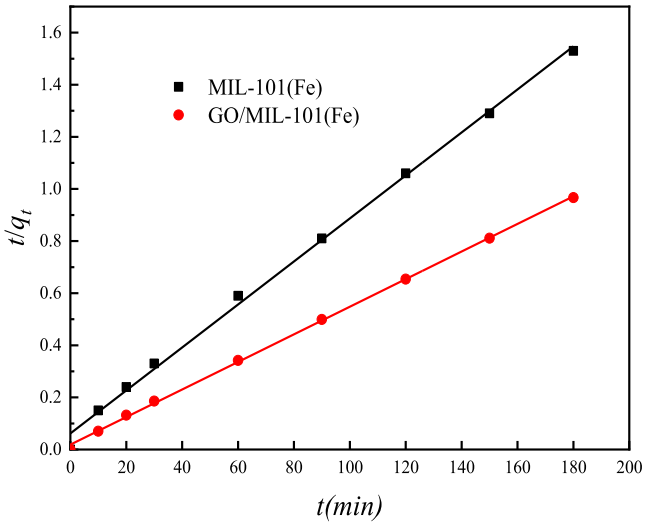

Figure 10. Pseudo-second-order kinetic curves for MO adsorption onto MIL-101(Fe) and GO/MIL-101(Fe).

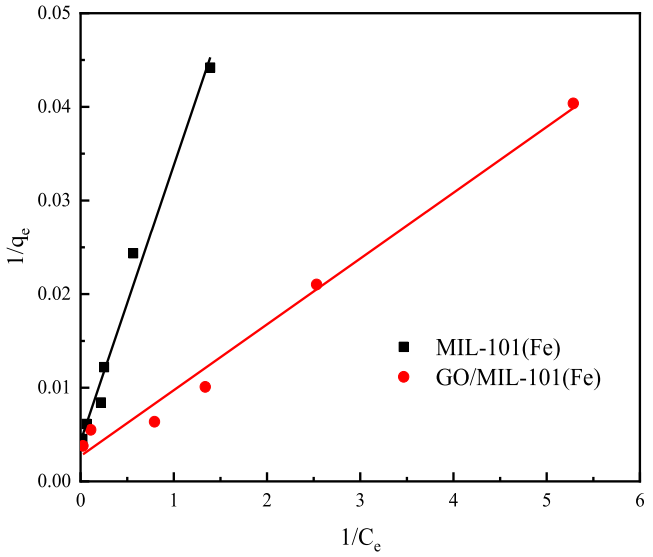

Figure 11. Adsorption isotherms for MO onto MIL-101(Fe) and GO/MIL-101(Fe) at 298 K.

pseudo-second order to be the best fit model, and it was confirmed that the removal of methyl orange by GO/MIL-101(Fe) was mainly based on the chemical reaction between GO/MIL-101(Fe) and MO.

3.4. Adsorption Isotherm. The adsorption isotherms of MIL-101(Fe) and GO/MIL-101(Fe) for the adsorption of MO are shown in Figure 11. It can be seen from Figure 11 that the adsorption capacity of 10% GO/MIL-101(Fe) for MO is significantly higher than that of MIL-101(Fe). The experimental data were fitted using the Langmuir and Freundlich adsorption isotherm equations.

The Langmuir adsorption isotherm model is given as follows

$$\frac{1}{q_e} = \frac{1}{Q^0} + \left(\frac{1}{bQ^0}\right)\left(\frac{1}{C_e}\right) \quad (4)$$

where Q^0 is the amount of monomolecular layer-saturated adsorption ($mg{\cdot}g^{-1}$) and b is the Langmuir equilibrium constant. Q^0 and b can be calculated from the slope and intercept of the straight-line plot of $1/q_e$ versus $1/C_e$.

The Freundlich adsorption isotherm model is represented as follows

$$\log q_e = \log K_F + \frac{1}{n}\log C_e \quad (5)$$

The Langmuir and Freundlich isothermal adsorption models were used to fit the adsorption data of MIL-101(Fe) and GO/MIL-101(Fe) adsorbents for the methyl orange simulation solution. The fitting results are shown in Figure 11 and Table 4. The linear correlation coefficients R^2 of the Langmuir adsorption isotherm model fitting were 0.983 and 0.986, respectively, which were greater than the linear correlation coefficients R^2 of the Freundlich adsorption isotherm model fitting, indicating that the adsorption process of MIL-101(Fe) and GO/MIL-101(Fe) for methyl orange was based on the Langmuir adsorption isotherm model. Accordingly, the adsorption of methyl orange by the adsorbent was monolayer adsorption.

3.5. Effect of pH Values on Adsorption Performance. Figure 12 reveals the effects of pH values on the adsorption of MO onto MIL-101(Fe) and GO/MIL-101. The adsorption of both MIL-101(Fe) and GO/MIL-101 for MO increased when pH values were between 2 and 4 and then decreased gradually as the pH value increased. Under faintly acidic conditions, the adsorption capacity of MO was better due to the positive charge on the surface of the adsorbent since MO is an anionic dye. Under weakly acidic conditions, a protonation reaction occurred on the surface of the adsorbent.[32] As the pH value increased, OH^- in the solution increased consequently and competed with the anionic methyl orange, which decreased the adsorption capacity. At the same pH value, the adsorption of MO onto GO/MIL-101(Fe) was significantly higher than that onto MIL-101(Fe). The ζ-potential values of GO/MIL-101(Fe) at various pH values are shown in Figure 13. Under acidic conditions, more positive charges appeared on the surface of the composite and were attributed to the adsorbed MO.[37] With the increase of the pH value, the adsorption capacity of MO on GO/MIL-101(Fe) was reduced, as the anionic methyl orange in aqueous solution was repulsed by the negative charge on the surface of GO/MIL-101(Fe).[22]

3.6. Effect of Dosage on Adsorption Performance. Figure 14 demonstrates the effects of dosage on the adsorption of MO onto MIL-101(Fe) and GO/MIL-101(Fe). It can be seen that with the increase of dosage, the adsorption amount of methyl orange on MIL-101(Fe) and GO/MIL-101(Fe)

Table 3. Kinetic Model Parameters for MO Adsorption onto MIL-101(Fe) and GO/MIL-101(Fe) (pH = 7, C_0 = 100 $mg{\cdot}L^{-1}$, T = 298 K, and m = 0.05 g)

		Lagergren first order			pseudo-second order		
sample	q_e ($mg{\cdot}g^{-1}$)	k_1 (min^{-1})	$q_{e,c}$ ($mg{\cdot}g^{-1}$)	R^2	k_2 ($g{\cdot}mg^{-1}{\cdot}min^{-1}$)	$q_{e,c}$ ($mg{\cdot}g^{-1}$)	R^2
MIL-101(Fe)	117.74	0.0249	72.62	0.9603	0.0011	121.21	0.9970
GO/MIL-101(Fe)	186.20	0.0289	79.13	0.9338	0.0015	188.68	0.9993

https://dx.doi.org/10.1021/acsomega.0c05091
ACS Omega 2021, 6, 4597−4608

Table 4. Isotherm Parameters of MO Adsorption onto MIL-101(Fe) and GO/MIL-101(Fe) (298 K)

	Langmuir			Freundlich		
samples	Q^0 (mg·g^{-1})	b (L·mg^{-1})	R^2	K_F	N	R^2
MIL-101(Fe)	232.55	0.146	0.983	34.012	1.83	0.924
GO/MIL-101(Fe)	369.00	0.385	0.986	64.183	1.84	0.936

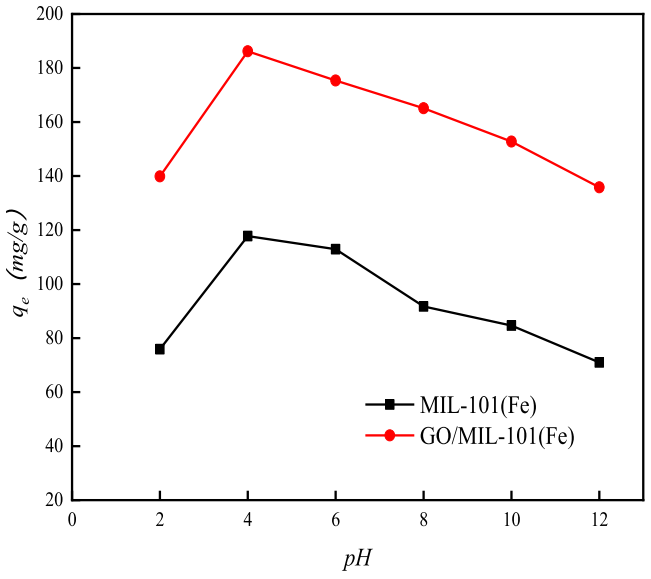

Figure 12. Effect of pH on the adsorption of MO onto MIL-101(Fe) and GO/MIL-101(Fe).

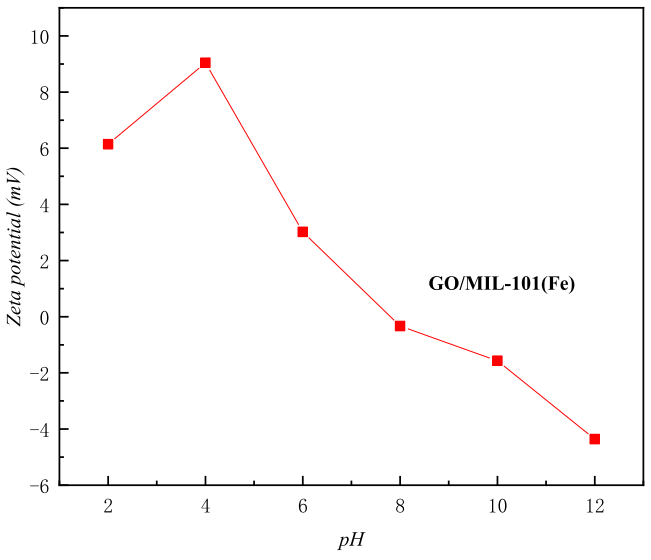

Figure 13. ζ-potential values of GO/MIL-101(Fe) at various pH values.

adsorbents gradually decreased. Due to the increase of dosage, the specific surface area and active adsorption sites provided by the adsorbent increased but the amount of the adsorbate (MO) in the solution remained constant; however, the unit adsorption capacity decreased with the increase of dosage. Within the chosen dosage range (0.05, 0.07, 0.09, 0.11, 0.13, and 0.15 g) in the study, the maximum adsorption capacity was found to be 0.05 g.

3.7. Effect of Temperature on Adsorption. The adsorption capacities of MO onto MIL-101(Fe) and GO/MIL-101(Fe) at different temperatures are shown in Figure 15.

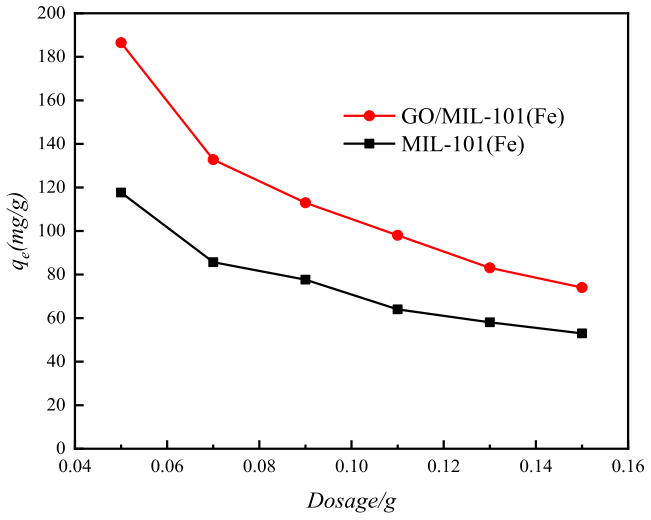

Figure 14. Effect of dosage on the adsorption of MO onto MIL-101(Fe) and GO/MIL-101(Fe).

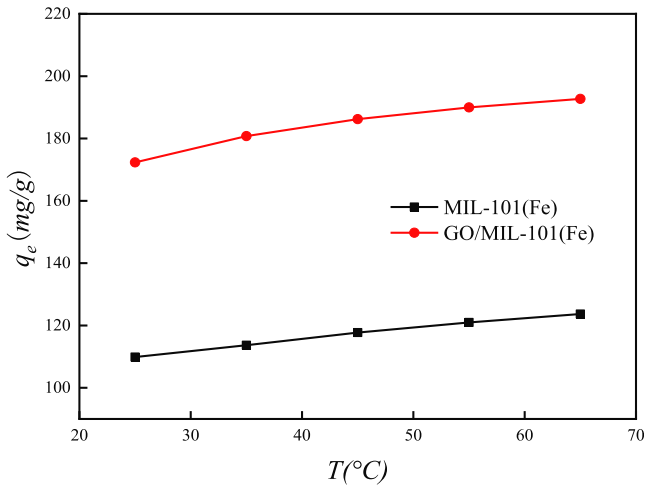

Figure 15. Effect of temperature on the adsorption of MO.

As can be seen, with the increase of temperature, the equilibrium adsorption capacity of MIL-101(Fe) and GO/MIL-101(Fe) adsorbents for methyl orange increased slightly, which indicated that the adsorption of methyl orange onto the adsorbents was an endothermic reaction and the effect of temperature on the adsorption of MO onto the two adsorbents was negligible.

The related thermodynamic parameters for MO adsorption onto GO/MIL-101(Fe) can be calculated from the following equation

$$\Delta G = \Delta H - T\Delta S \quad (6)$$

$$K_d = \frac{Q_e}{C_e} \quad (7)$$

https://dx.doi.org/10.1021/acsomega.0c05091
ACS Omega 2021, 6, 4597−4608

Table 5. Thermodynamic Parameters for MO Adsorption onto MIL-101(Fe) and GO/MIL-101(Fe)

samples	T/K	ΔG (kJ·mol^{-1})	ΔH (kJ·mol^{-1})	ΔS (J·K·mol)$^{-1}$)
MIL-101(Fe)	298.15	−2.82	2.24	9.46
	308.15	−2.91		
	318.15	−3.02		
	328.15	−3.13		
	338.15	−3.21		
GO/MIL-101(Fe)	298.15	−5.82	4.08	19.51
	308.15	−6.01		
	318.15	−6.23		
	328.15	−6.39		
	338.15	−6.59		

$$\log K_d = \frac{\Delta S}{R} - \frac{\Delta H}{2.303RT} \quad (8)$$

where ΔG is the change in the Gibbs free energy (J·mol^{-1}); ΔH is the change in apparent enthalpy (J·mol^{-1}); ΔS is the change in entropy (J K^{-1}·mol^{-1}); T is the thermodynamic temperature of the reaction (K); R is the universal gas constant, 8.314 (J·K^{-1}·mol^{-1}); K_d is the partition coefficient; Q_e is the equilibrium adsorption capacity (mg·g^{-1}); and C_e is the equilibrium concentration of the adsorbate (mg·L^{-1}).

The related thermodynamic parameters of MIL-101(Fe) and GO/MIL-101(Fe) adsorbents for methyl orange are presented in Table 5. It can be seen from Table 5 that the ΔH values of the methyl orange adsorption process of MIL-101(Fe) and GO/MIL-101(Fe) adsorbents are positive, illustrating that the adsorption process was an endothermic reaction process. ΔG is negative at different temperatures, showing that the adsorption was a spontaneous process. ΔS is a positive value, indicating that after the adsorption of methyl orange on the surfaces of MIL-101(Fe) and GO/MIL-101(Fe) adsorbents, the internal disorder of the reaction system increased during the adsorption process.

3.8. Reusability of the Adsorbent. After the adsorption process, the composite was obtained from aqueous solution by centrifugation and then added into 100 mL of ethanol and shaken for 30 min; this step was repeated three times till the supernatant of the solution was nearly colorless. The adsorbent was washed repeatedly by deionized water, dried in an oven at 70 °C, and finally activated in a vacuum drier at 150 °C for 10 h for the next experiment. The results of the desorption experiments of the MIL-101(Fe) and GO/MIL-101(Fe) adsorbents are shown in Figure 16. It can be seen from Figure 16 that after three adsorption cycles, the adsorption of methyl orange by the MIL-101(Fe) adsorbent decreased from 117.4 to 79.87 mg·g^{-1}, and the adsorption amount of MO by the GO/MIL-101(Fe) adsorbent decreased from 186.2 to 130.03 mg·g^{-1}. The results showed that after three reuses, the MIL-101(Fe) and GO/MIL-101(Fe) adsorbents still maintained a high adsorption capacity for methyl orange, which indicated that their regeneration performance was good. This phenomenon of the decrease may be due to the fact that part of the methyl orange molecules entered GO/MIL-101(Fe) during the adsorption process; besides, these methyl orange molecules could not be washed out from the pores during the regeneration washing process. Therefore, regeneration of the adsorption sites occurred almost on the surface of the adsorbent in each regeneration washing. Meanwhile, the adsorption of MO onto adsorbents from other studies is given in Table 6.

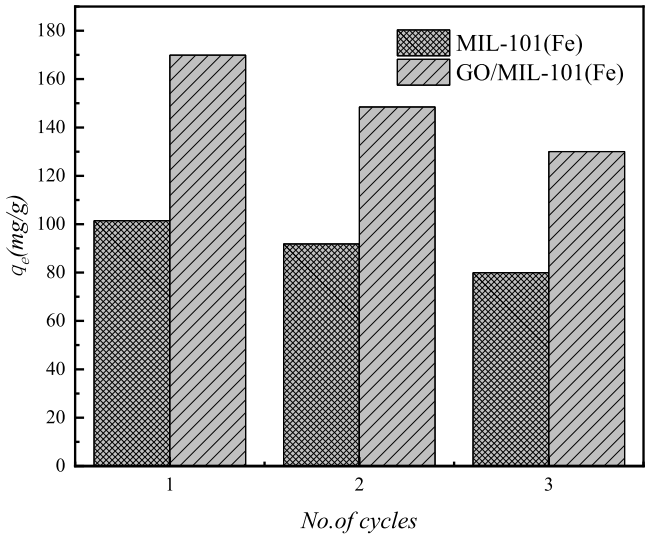

Figure 16. Results of desorption regeneration of adsorbents.

Table 6. Adsorption Capacities of Different Adsorbents for the Removal of MO from Aqueous Solution

adsorbent	adsorption capacity (mg·g^{-1})	reference
polyaniline based on DBSNa	75.9	39
MIL-53(Al)	81.2	40
graphene oxide aerogel (GOA)	55.56	41
$CoFe_2O_4$/GO	33.85	42
GO-IPDI-CDs	83.40	43
QPEI/SiO_2	105.4	44
MS_Br@AC40	123.20	45
MIL-101(Fe)/GO	186.2	in this work

3.9. Adsorption Mechanism. The adsorption mechanism is presented in Figure 17. GO agglomerates in the reaction system that may prevent the organic ligands to coordinate with Fe^{3+} ions and more positive charges appear on the surface of the composites material. The adsorption capacity of the composite for MO was improved through electrostatic attraction[46] between the positive charge on the surface of GO/MIL-101(Fe) and the negative charge of the sulfonic acid group of MO, and the electronegative N atom of MO interacted with Fe ions by the complexing reaction. The carboxyl and hydroxy groups on the surface of GO or the carboxyl groups of terephthalic acid interacted with MO by hydrogen bonding.[32] MO also may adsorb on the surface of the composite by $\pi-\pi$ stacking.[47]

https://dx.doi.org/10.1021/acsomega.0c05091
ACS Omega 2021, 6, 4597−4608

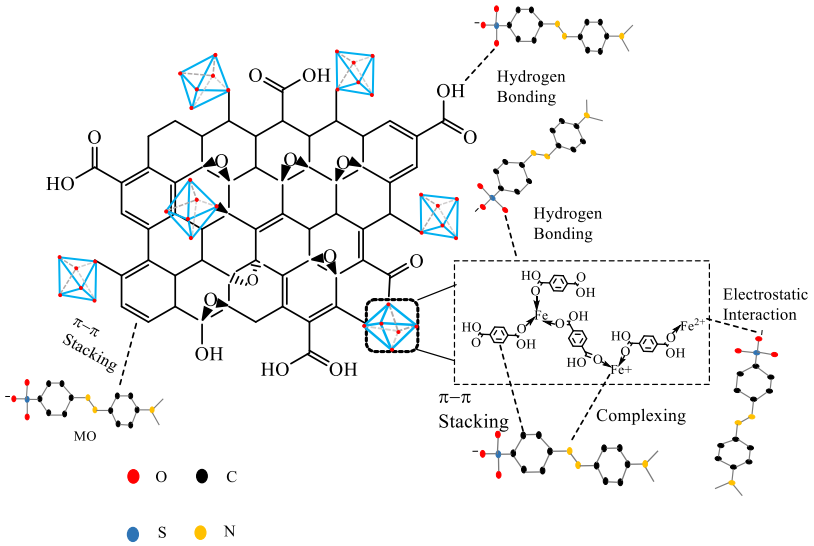

Figure 17. Adsorption mechanism of MO onto GO/MIL-101(Fe).

4. CONCLUSIONS

In this paper, GO/MIL-101(Fe) was prepared by doping MIL-101(Fe) with graphene oxide. The MIL-101(Fe) material can maintain its polyhedron structure and grow on the surface of the GO single layer, which formed the structure of GO/MIL-101(Fe). The surface area of GO/MIL-101(Fe) decreased due to blockage of a part of GO in the composite, but its active sites increased; therefore, GO agglomerated in the reaction system that may prevent the organic ligands to coordinate with Fe^{3+} ions and more positive charges appeared on the surface of the composite material. Thus, the maximum adsorption capacity of GO/MIL-101(Fe) was better than MIL-101(Fe) for MO, and the maximum adsorption capacities of MILL-101(Fe) and GO/MIL-101(Fe) were 117.74 and 186.20 mg·g^{-1}, respectively. Its adsorption behavior was more consistent with the Langmuir adsorption isotherm equation. Adsorption kinetics data ascertained the pseudo-secondary kinetic model, and the adsorption process to MO was a spontaneous endothermic reaction. GO/MIL-101(Fe) exhibits good regeneration ability, which can be reused at least three times. This study showed that GO/MIL-101(Fe) is a good candidate for the removal of organic pollutants from wastewater.

AUTHOR INFORMATION

Corresponding Author

Wenwen He − *College of Geology and Environment, Xi'an University of Science and Technology, Xi'an 710054, China;* orcid.org/0000-0002-9504-7893; Phone: +8618792531404; Email: 1319994921@qq.com

Authors

Zhuannian Liu − *College of Geology and Environment, Xi'an University of Science and Technology, Xi'an 710054, China*

Qingyun Zhang − *College of Geology and Environment, Xi'an University of Science and Technology, Xi'an 710054, China*

Habiba Shapour − *College of Geology and Environment, Xi'an University of Science and Technology, Xi'an 710054, China*

Mohammad Fahim Bakhtari − *College of Geology and Environment, Xi'an University of Science and Technology, Xi'an 710054, China*

Complete contact information is available at: https://pubs.acs.org/10.1021/acsomega.0c05091

Author Contributions

Conceptualization, resource, and methodology were performed by Z.L.; investigation was done by H.W.; software and data curation was performed by Z.Q.; writing-original draft preparation and writing-review and editing was done by H.W.; language was checked and validated by H.S.; and language was also checked by M.F.B.

Notes

The authors declare no competing financial interest.

ACKNOWLEDGMENTS

The authors greatly appreciate financial support from the General Project of the National Natural Science Foundation of China: Preparation of coal/polyethyleneimine cross-linked complex chelating adsorbent and its mechanism of synergistic effect on heavy metal ions (No. 51278418)

REFERENCES

(1) Hou, Y. R.; Yan, S. N.; Huang, G. G.; Yang, Q. P.; Huang, S. R.; Cai, J. J. Fabrication of N-doped carbons from waste bamboo shoot shell with high removal efficiency of organic dyes from water. *Bioresour. Technol.* **2020**, *303*, No. 122939.

(2) Tkaczyk, A.; Mitrowska, K.; Posyniak, A. Synthetic organic dyes as contaminants of the aquatic environment and their implications for ecosystems: A review. *Sci. Total Environ.* **2020**, *717*, No. 137222.

(3) Azam, K.; Raza, R.; Shezad, N.; Shabir, M.; Yang, W.; Ahmad, N.; Shafiq, I.; Akhter, P.; Razzaq, A.; Hussain, M. Development of recoverable magnetic mesoporous carbon adsorbent for removal of methyl blue and methyl orange from wastewater. *J. Environ. Chem. Eng.* **2020**, *8*, No. 104220.

(4) Liu, S. T.; Wang, W. Z.; Cheng, Y.; Yao, L. Z.; Han, H. S.; Zhu, T. Y.; Liang, Y. J.; Fu, J. L. Methyl orange adsorption from aqueous solutions on 3D hierarchical PbS/ZnO microspheres. *J. Colloid Interface Sci.* **2020**, *574*, 410−420.

(5) Chiang, C.-H.; Chen, J.; Lin, J. H. Preparation of pore-size tunable activated carbon derived from waste coffee grounds for high adsorption capacities of organic dyes. *J. Environ. Chem. Eng.* **2020**, *8*, No. 103929.

(6) Mantasha, I.; Saleh, H. A. M.; Qasem, K. M. A.; Shahid, M.; Mehtab, M.; Ahma, M. Efficient and selective adsorption and separation of methylene blue (MB) from mixture of dyes in aqueous

environment employing a Cu(II) based metal organic framework. *Inorg. Chim. Acta.* **2020**, *511*, No. 119787.
(7) Pedrazzo, A. R.; Smarra, A.; Cladera, F.; Musso, G.; Dhakar, N. K.; Cecone, C.; Hamedi, A.; Corsi, I.; Trotta, F. Eco-friendly beta-cyclodextrin and linecaps polimers for removal of Heavy metals. *Polymers* **2019**, *10*, No. 1658.
(8) Zhu, Y.; Fan, W. H.; Zhou, T. T.; Li, X. M. Removal of chelated heavy metals from aqueous solution: A review of current methods and mechanisms. *Sci. Total Environ.* **2019**, *678*, 253−266.
(9) Pham, T.; Forrest, K. A.; Franz, D. M.; Space, B. Experimental and theoretical investigations of the gas adsorption sites in rht-metal-organic frameworks. *CrystEngComm* **2017**, *19*, 4646−4665.
(10) Corma, A.; Garcia, H.; Xamena, F. X. L. I. Engineering metal organic frameworks for heterogeneo us catalysis. *Chem. Rev.* **2010**, *110*, 4606−4655.
(11) Liu, Z. B.; Chen, Y.; Sun, J. H.; Lang, H. W.; Gao, W. Q.; Chi, Y. Y. Amine grafting on coordinatively unsaturated metal centers of MIL-101(Cr) for improved water absorption characteristics. *Inorg. Chim. Acta* **2018**, *473*, 29−36.
(12) Zango, Z. U.; Bakar, N. H. H. A.; Sambudi, N. S.; Jumbri, K.; Abdullah, N. A. F.; Abdul Kadir, E.; Saad, E. Adsorption of chrysene in aqueous solution onto MIL-88(Fe) and NH2-MIL-88(Fe) metal-organic frameworks: Kinetics, isotherms, thermodynamics and docking simulation studies. *J. Environ. Chem. Eng.* **2020**, *8*, No. 103544.
(13) Khudozhitkov, A. E.; Arzumanov, S. S.; Kolokolov, D.; Stepanov, A. G. Dynamics of xylene isomers in MIL-53 (Al) MOF probed by solid state 2IH NMR. *Microporous Mesoporous Mater.* **2020**, *30*, No. 110155.
(14) Sun, S. W.; Yang, Z. H.; Cao, J.; Wang, Y.; Xiong, W. P. Copper-doped ZIF-8 with high adsorption performance for removal of tetracycline from aqueous solution. *J. Solid. State. Chem.* **2020**, *285*, No. 121219.
(15) Chen, T.; Wang, P. F.; Du, X.; Gao, F. F.; Ma, X. L.; Liu, F. F.; Alameen, A.; Tang, K. Y.; Hao, X. G. A novel hexagonal prism Cu-BTC by unipolar pulse electropolymerization. *Mater. Lett.* **2019**, *254*, 137−140.
(16) He, H. B.; Li, R.; Yang, Z. H.; Chai, L. Y.; Jin, L. F.; Alhassan, S. I.; Ren, L. L.; Wang, H. Y.; Huang, L. Preparation of MOFs and MOFs derived materials and their catalytic application in air pollution: A review. *Catal. Today.* **2020**, 1−19, DOI: 10.1016/j.cattod.2020.02.033.
(17) Hamedi, A.; Caldera, F.; Trotta, F.; Zarandi, M. B.; Pedrazzo, A. R.; Claudio, C. Metal organic frameworks in medicine. *Acta. Sci. Pharma. Sci.* **2019**, *4*, 107−109.
(18) Kholdeeva, O. A.; Skobelev, I. Y.; Ivanchikova, I. D.; Kovalenko, K. A.; Fedin, V. P.; Sorokin, A. B. Hydrocarbon oxidation over Fe- and Cr-containing metal-organic frameworks MIL-100 and MIL-101−a comparative study. *Catal. Today.* **2014**, *238*, 54−61.
(19) Thanh, H. T. M.; Phuong, T. T. T.; Hang, P. T. L.; Toan, T. T. T.; Tuyen, T. N.; Mau, T. X.; Khieu, D. Q. Comparative study of Pb(II) adsorption onto MIL−101 and Fe−MIL−101 from aqueous solutions. *J. Environ. Chem. Eng.* **2018**, *6*, 4093−4102.
(20) Li, Z. C.; Liu, X. M.; Jin, W.; Hu, Q. S.; Zhao, Y. P. Adsortion behavior of arsenicals on MIL-101(Fe): The role of arsenic chemical structures. *J. Colloid Interface Sci.* **2019**, *554*, 692−704.
(21) Hamedi, A.; Zarandi, M. B.; Nateghi, M. R. Highly efficient removal of dye pollutants by MIL-101(Fe) metal-organic framework loaded magnetic particles mediated by poly L-Dopa. *J. Environ. Chem. Eng.* **2019**, *7*, No. 102882.
(22) Hamedi, A.; Trotta, F.; Borhani Zarandi, M.; Zanetti, M.; Caldera, F.; Anceschi, A.; Nateghi, M. R. In situ synthesis of MIL-101(Fe) at the surface of Fe3O4@AC as highly efficient dye adsorbing nanocomposite. *Int. J. Mol. Sci.* **2019**, *22*, No. 5612.
(23) Zhu, T. Y.; Xu, S.; Yu, F.; Yu, X.; Wang, Y. ZIF-8@GO composites incorporated polydimethylsiloxane membrane with prominent separation performance for ethanol recovery. *J. Membr. Sci.* **2020**, *598*, No. 117681.
(24) Li, Y. Q.; Umer, R.; Samad, Y. J. A.; Zheng, L. X.; Liao, K. The effect of the ultrasonication pre-treatment of grapheme oxide(GO) on the mechanical properties of GO/polyvinyl alcohol composites. *Carbon* **2013**, *55*, 321−327.
(25) Sahoo, S. K.; Tripathy, M.; Hota, G. In-situ functionalization of GO sheets with ALOOH-FeOOH composite nanorods: An eco-friendly annoadsorbent for removal of toxic arsenate ions from water. *J. Environ. Chem. Eng.* **2019**, *7*, No. 103357.
(26) Dahaghin, Z.; Kilmartin, P. A.; Mousavi, H. Z. Simultaneous determination of lead(II) and cadm-ium(II) at a glassy carbon electrode modified with GO@Fe_3O_4@benzothiazole-2-carboxaldehyde using square wave anodic stripping voltammetry. *J. Mol. Liq.* **2018**, *249*, 1125−1132.
(27) El-Shafai, N. M.; Abdelfatah, M. M.; El-Khouly, M. E.; El-Mehasseb, I. M.; El-Shaer, A.; Ramadan, M. S.; Masoud, M. S.; El-Kemary, M. A. Magnetitle nano-spherical quantum dots decorated grapheme oxide nano sheet (GO@Fe_3O_4): Electrochemical properties and application for removal heavy metals, pesticide, and solar cell. *Appl. Surf. Sci.* **2020**, *506*, No. 144896.
(28) Jia, X. N.; Zhao, P.; Ye, X.; Zhang, L. J.; Wang, T.; et al. A novel metal-organic framework composite MIL-101(Cr)@GO as an efficient sorbent in dispersive micro-solid phase extraction coupling with UHPLC-MS/MS for the determination of sulfonamides in milk samples. *Talanta* **2017**, *169*, 227−238.
(29) Li, Y. J.; Miao, J. P.; Sun, X. J.; Xiao, J.; Li, Y. W.; Wang, H. H.; Xia, Q. B.; Li, Z. Mechanochemical synthesis of Cu-BTC@GO with enhanced water stability and toluene adsorption capacity. *Chem. Eng. J.* **2016**, *298*, 191−197.
(30) Barbosa, A. D. S.; Julião, D.; Fernandes, D. M.; Peixoto, A. F.; Freire, C.; Castro, B.; Granadeiro, C. M.; Balula, S. S.; Silva, L. C. Catalytic performance and electrochemical behaviour of Metal−organic frameworks: MIL-101(Fe) versus NH2-MIL-101(Fe). *Polyhedron* **2017**, *127*, 464−470.
(31) Zhang, J.; Li, Z.; Qi, X. L.; Zhang, W.; Wang, D. Y. Size tailored bimetallic metal-organic framework (MOF) on grapheme oxide with sandwich-like structure as functional nano-hybrids for improving fire safety of epoxy. *Composites Engineering* **2020**, *188*, No. 107881.
(32) Luo, S. L.; Xu, X. L.; Zhou, G. Y.; Liu; Tang, Y. H.; Liu, Y. T. Amino siloxane oligomer-linked graphene oxide as an efficient adsorbent for adsorbent for removal of Pb(II) from wastewater. *J. Hazard. Mater.* **2014**, *274*, 145−155.
(33) Gao, J.; He, P.; Yang, T. T.; Wang, X. J.; Zhou, L. H.; He, Q. H.; Jia, L. P.; Deng, H. Q.; Zhang, H.; Jia, B.; He, X. C. Short rod-like Ni-MOF anchored on graphene oxide nanosheets: A promising Voltammetric platform for highly sensitive determination of pchloronitrobenzene. *J. Electroanal. Chem.* **2020**, *861*, No. 113954.
(34) Nebol'sin, V. A.; Galstyan, V.; Silina, Y. E. Graphene oxide and its chemical nature: Multi-stage interractions between the oxygen and graphene. *Surf. Interfaces.* **2020**, *21*, No. 100763.
(35) Yang, S. J.; Zou, Q. F.; Wang, T. H.; Zhang, L. P. Effects of GO and MOF@GO on the permeation and antifouling properties of cellulose acetate ultrafiltration membrance. *J. Mem. Brane. Sci.* **2019**, *569*, 46−59.
(36) Ullah, S.; Bustam, M. A.; Al-Sehemi, A. G.; Assiri, M. A.; Abdul-Kareem, F. A.; Mukhtar, A.; Ayoub, M.; Gonfa, G. Influence of post-synthetic graphene oxide(GO) functionalization on the selective CO2/CH4 adsorption behavior of MOF-200 at different temperatures; an experimental and adsorption isotherms study. *Microporous Mesoporous Mater.* **2020**, *296*, No. 110002.
(37) Chaturvedi, G.; Kaur, A.; Umar, A.; Khan, M. A.; Algarni, H.; Kansal, S. B. Removal of fluoroquinolone drug, levofloxacin, from aqueous phase over iron based MOFs, MIL-101(Fe). *J. Solid State Chem.* **2020**, *281*, No. 121029.
(38) Li, Z. C.; Liu, X. M.; Jin, w.; Hu, Q. S.; Zhao, Y. P. Adsorption behavior of arsenicals on MIL-101(Fe): The role of arsenic chemical structures. *J. Colloid Interface Sci.* **2019**, *554*, 692−704.
(39) Karri, R. R.; Tanzifi, M.; Yaraki, M. T.; Sahu, J. N. Optimization and modeling of methyl orange adsorption onto polyaniline nano-adsorbent through response surface methodology and differential

https://dx.doi.org/10.1021/acsomega.0c05091
ACS Omega 2021, 6, 4597−4608

evolution embedded neural network. *J. Environ. Mange.* **2018**, *223*, 517−529.
(40) Al Sharabati, M.; Sabouni, R. Selective removal of dual dyes from aqueous solutions using a metal organic framework (MIL-53(Al)). *Polyhedron* **2020**, *190*, No. 114762.
(41) Tu, T. H.; Cam, P. T. N.; Huy, L. V. T.; Phong, M. T.; Nam, H. M.; Hieu, N. H. Synthesis and application of graphene oxide aerogel as an adsorbent for removal of dyes from water. *Mater. Lett.* **2019**, *238*, 134−137.
(42) Chang, S. C.; Zhang, Q.; Lu, Y. K.; Wu, S. Z.; Wang, W. High-efficiency and selective adsorption of organic pollutants by magnetic CoFe2O4/graphene oxide adsorbents: Experimental and molecular dynamics simulation study. *Sep. Purif. Technol.* **2020**, *238*, No. 116400.
(43) Yan, J.; Zhu, Y.; Qiu, F. X.; Zhao, H.; Yang, D. Y.; Wang, J.; Wen, W. Y. Kinetic, isotherm and thermodynamic studies for removal of methyl orange using a novel β-cyclodextrin functionalized graphene oxide-isophorone diisocyanate composites. *Chem. Eng. Res. Des.* **2016**, *106*, 168−177.
(44) Liu, J. S.; Ma, S.; Zang, Lj. Preparation and characterization of ammonium-functionalized silica nanoparticle as a new adsorbent to remove methyl orange from aqueous solution. *Appl. Surf. Sci.* **2013**, *265*, 393−398.
(45) Pargoletti, E.; Pifferi, V.; Falciola, L.; Facchinetti, G.; Depaolini, A. R.; Davoli, E.; Marelli, M.; Cappelletti, G. A detailed investigation of MnO2 nanorods to be grown onto activated carbon. High efficiency towards aqueous methyl orange adsorption/degradation. *Appl. Surf. Sci.* **2019**, *472*, 118−126.
(46) Wang, Y.; Zhou, R. S.; Wang, C. Z.; Zhou, G. Z.; Hua, C. Y.; Cao, Y. Y.; Song, Z. Z. Novel environmental-friendly nano-composite magnetic attapulgite functionalized by chitosan and EDTA for cadmium(II) removal. *J. Alloys Compd.* **2020**, *817*, No. 153286.
(47) Tian, J.; Wu, S.; Yin, X. L.; Wu, W. Novel preparation og hydrophilic graphene/graphene oxide nanosheets for supercapacitor electrode. *Appl. Surf. Sci.* **2019**, *496*, No. 143696.

https://dx.doi.org/10.1021/acsomega.0c05091
ACS Omega 2021, 6, 4597−4608